Steps toward interstellar silicate mineralogy. IV The crystalline revolution

Jager, C.; Molster, F.J.; Dorschner, J.; Henning, T.; Mutschke, H.; Waters, L.B.F.M.

Published in:
Astronomy & Astrophysics

Astron. Astrophys. 339, 904–916 (1998)

ASTRONOMY AND ASTROPHYSICS

Steps toward interstellar silicate mineralogy

IV. The crystalline revolution

C. Jäger[1], F.J. Molster[2], J. Dorschner[1], Th. Henning[1], H. Mutschke[1], and L.B.F.M. Waters[2,3]

[1] Astrophysical Institute and University Observatory (AIU), Schillergässchen 2-3, D-07745 Jena, Germany
[2] Astronomical Institute 'Anton Pannekoek', University of Amsterdam, Kruislaan 403, 1098 SJ Amsterdam, The Netherlands
[3] SRON Space Research Laboratory, P.O. Box 800, 9700 AV Groningen, The Netherlands

Received 23 April 1998 / Accepted 19 June 1998

Abstract. Mid- and far-infrared spectra gained by the Short Wavelength Spectrometer (SWS) of the Infrared Space Observatory (ISO) satellite have provided striking evidence for the presence of crystalline silicates in comets, circumstellar envelopes around young stars and, most of all, evolved stars and planetary nebulae. Since optical properties of astrophysically relevant crystalline silicates are lacking in the literature, in this paper mass absorption coefficients (MACs) of olivines and pyroxenes for a wide range of Mg/Fe ratios are presented, which cover the whole ISO wavelength range . The MAC have been derived from transmission spectra of small grains embedded in potassium bromide and polyethylene pellets. Only in the case of natural enstatite ($MgSiO_3$), was a monocrystalline sample available, which allowed the measurement of optical constants for the different crystallographic orientations of this anisotropic silicate. Since not all Mg/Fe ratios are represented among the natural minerals, we supplemented the series by synthetic products prepared in our lab. We also included two inhomogeneous synthetic materials, one of olivine and the other one of pyroxene composition, which are expected to be similar to the primary condensate in cosmic environments.

For all samples the chemical composition, the purity, and the homogeneity have been determined by energy-dispersive X-ray analysis and by scanning electron microscopy. Especially for the minerals, it is important to exclude the spectral influence of differently composed inclusions.

The peak positions of the samples are influenced by different factors which are discussed: chemical composition (FeO content), size and shape distribution of the grains, and the matrix in which the grains are embedded for spectroscopy.

The continuum-subtracted ISO SWS spectrum of the source AFGL 4106 has been compared with simple optically thin model spectra calculated for our olivine and pyroxene samples. The main result was that a combination of the pure magnesium silicates (forsterite and enstatite) gives a good agreement between observations and laboratory measurements.

Key words: line: identification – methods: laboratory – circumstellar matter – infrared: ISM: lines and bands – infrared: stars

Send offprint requests to: C. Jäger

1. Introduction

Before the Infrared Space Observatory (ISO, Kessler et al. 1996) opened the mid- and far-infrared range for high-resolution spectroscopy, it was generally assumed that cosmic dust silicates were of amorphous structure. Exceptions were the cometary dust (Hanner et al. 1994, Hanner 1996), interplanetary dust particles (IDPs, Mackinnon & Rietmeijer 1987, Bradley et al. 1992), dust disks of β Pictoris-type around main-sequence stars (Knacke et al. 1993, Fajardo-Acosta & Knacke 1995), and the deeply embedded young stellar object AFGL 2591 (Aitken et al. 1988). This assumption was apparently confirmed by the shapes of the observed silicate vibrational bands at about 10 and 19 μm (Dorschner & Henning 1986, 1995, Dorschner 1997) as well as by non-equilibrium condensation experiments providing "chaotic silicates" (Nuth 1996). Therefore, laboratory studies were mainly concentrated on the glassy silicates of supposed cosmic abundances, e.g. in the Jena Laboratory Astrophysics Group efforts have been focused on producing, characterizing, and measuring glasses with the aim to provide their optical constants over the whole astrophysically relevant wavelength range (Jäger et al. 1994, Dorschner et al. 1995, Mutschke et al. 1997). In addition, measurements of optical properties at low temperatures were performed (Henning & Mutschke 1997).

However, when the first ISO SWS spectra became available, one of the most surprising discoveries was the finding of clear evidence of crystalline silicates. The presence of at least a portion of crystalline silicates was found in the spectra of comet Hale-Bopp (Crovisier et al. 1997), circumstellar dust around Herbig Ae/Be stars (Waelkens et al. 1996), low-mass evolved stars with high mass loss including planetary nebulae (Waters et al. 1996; Justtanont et al. 1996) and Luminous Blue Variables (LBVs) (Waters et al. 1997).

In contrast to chaotic silicates and silicate glasses, crystalline silicates show a lot of diagnostic bands due to metal-oxygen vibrations in the mid-infrared (MIR) range beyond 17 μm. This promises at least the possibility to derive values of the Mg/Fe ratio of crystalline silicates. Generally, we would learn more about the formation process of the dust grains and the connection between amorphousness and crystallinity of stardust silicates.

The crystalline silicates mark their presence by narrow features on top of the continuum. Prominent emission and absorption features have been found in ISO spectra around 10.1, 11.2, 13.8, 16.3, 19.5, 21.5, 23.7, 27.9, 33.6, 35.5, 36.5, 40.5, 43.0, and 69.5 μm (Molster et al. in prep.), marking the presence of crystalline olivines and pyroxenes. Not in every case are all of these features visible, which may be explained by temperature effects, i.e. the convolution of the absorption coefficient with a Planck function can suppress features in spectral regions where the emitted radiation is low. The wavelengths of the peak positions can slightly change from source to source by 0.1-0.3 μm, while the widths of the bands vary more drastically. Both types of variation may be due to varying Fe/Mg-ratios within the same silicate type, blending of different silicates, the degree of crystallization and size/shape effects of the particles.

The spectral resolution of the ISO-SWS AOT01 spectra is relatively high for dust spectroscopy ($\lambda/\Delta\lambda \approx 1500$). In order to fully exploit the information on cosmic dust silicates contained in these ISO spectra, laboratory data of adequate spectral resolution covering the entire ISO wavelength range are urgently needed. Unfortunately, such spectral data of Mg-Fe silicates are very rare in the literature (see, e.g., Steyer 1974, Koike et al. 1993, Hofmeister 1997). It is the aim of this paper to provide additional data of crystalline olivine- and pyroxene-type silicates, which cover the whole wavelength range important for the interpretation of ISO spectra, and to study the influence of the Fe/Mg ratio on band positions and strength ratios. This investigation contains synthetic samples of the series end members $MgSiO_3$, Mg_2SiO_4, and Fe_2SiO_4 as well as natural orthopyroxenes and olivines (enstatite, bronzite, hypersthene, olivine, and hortonolite). We have measured the whole Mg/Fe compositional range for the olivines, but were only able to cover a part of this range for the pyroxenes. The spectroscopy is supplemented by a careful analytical characterization of the samples.

In the course of the characterization procedure of the samples, we found several pure and homogeneous silicates that can be used as reference materials for spectroscopy. Natural minerals often contain phase separations and inclusions of completely different materials which, in extreme cases, could dominate the "silicate" spectrum.

We also investigated synthetic silicates that were effectively quenched so that inhomogeneities developed. Rapid cooling of homogeneous melts of olivine and pyroxenes provides phase separation consisting of an SiO_2-rich and a metal oxide-rich component, comparable to the aforementioned "chaotic" silicates (Rietmeijer et al. 1986, Nuth 1996) suggested to be the primary nucleation products in the multi-component gas of oxygen-rich circumstellar envelopes.

Sect. 2 gives an overview about the composition and structure of crystalline silicates in the solid solution series of pyroxenes and olivines. Sect. 3 describes the exact chemical composition of the synthetic and natural silicates and other results of analytical studies of the samples. Sect. 4 deals with the results of the sample spectroscopy in the MIR and far infrared (FIR), discusses the spectral features and compares the results with previous measurements. We will also present optical constants of the natural enstatite determined from reflection measurements. In Sect. 5 the laboratory data are compared to the new ISO results on "crystalline" features, and other astrophysical implications are discussed.

2. Structure of crystalline silicates

The silicates studied in this paper belong to the mineral groups of olivines and pyroxenes. The olivine group consists of silicates with the general sum formula $A^{2+}B^{2+}SiO_4$. A and B are divalent cations, the most abundant of which are Mg, Fe, Mn, Co and Zn. In this paper we concentrate on the olivines in which the cations Mg^{2+} and Fe^{2+} dominate. They replace each other in the crystal: that means, these olivines can be considered as solid solutions of Mg_2SiO_4 and Fe_2SiO_4; the mixture ratio can be expressed by the subscript x with $0 \leq x \leq 1$ in the general formula $Mg_{2x}Fe_{2-2x}SiO_4$. The end members of the isomorphous series, Mg_2SiO_4 (x=1) and Fe_2SiO_4 (x=0), have the mineral names forsterite and fayalite, respectively. The mineral "olivine" contains 8 to 20 mass percent FeO. Minerals with higher FeO contents are called hortonolite and ferrohortonolite. The olivines are neso-silicates (island silicates) because they consist of isolated SiO_4 tetrahedra, the basic structural unit of all types of silicates, which are linked by divalent cations. The metal ions are coordinated by six oxygens. There are two nonequivalent six-coordinate positions in the olivine structure which are both distorted (Burns 1970). According to the lattice symmetry, the olivines belong to the rhombic crystal system. In the solid solution series of olivines, the increasing Fe incorporation leads to larger metal-oxygen distances in the crystal.

The pyroxenes form a large group of minerals belonging to the inosilicates (chain silicates). The two SiO_4 tetrahedra form $[Si_2O_6]_\infty$ chains, i.e. each tetrahedron shares two of its oxygens with the neighbours. However, in chemical sum formula often the simple expression $MeSiO_3$ is used (Me means metal ion). The direction of the chains is the crystallographic c-axis. Like in the case of the olivines, we focus our interest on pyroxenes with the cations Mg and Fe and use the symbolic formula $Mg_xFe_{1-x}SiO_3$. There are two types of SiO_4 tetrahedral chains with different Si-O distances. The metal ions in the Mg-Fe-pyroxenes linking the SiO_4 chains are coordinated by six oxygens. There are also two different types of distorted MeO_6 octahedra. Like in the case of the olivines the Me-O distances increase with growing FeO content. The pyroxenes also form solid solution series. The Fe-free and Mg-free end members are enstatite (x=1) and ferrosilite (x=0), respectively. In contrast to olivines, pyroxenes occur in two different main crystallographic systems. The lattice can be of rhombic or monoclinic structure. The rhombic crystal structure is produced by twinning of the unit cell of clinopyroxene by operation of a b-glide parallel to (100)-plane. Pyroxenes containing cations with radii considerably larger than that of Mg^{2+}, e.g. Ca^{2+}, belong to the monoclinic system and are called clinopyroxenes. Under extreme formation conditions, monoclinic Mg-Fe pyroxenes can also arise, e.g. clinoenstatite. Synthetic Mg pyroxenes produced via melting usually are of this type. However, Mg-Fe clinopy-

Table 1. Analytical results for the pure synthetic and natural silicate materials determined by EDX analysis; the symbol s means synthetic material, n stands for natural mineral. The last column contains the amount of minor oxide components (in mass %) and the kinds of inclusions.

Formula	**Mineral name**	**Composition (mass %)**			
		MgO	FeO	SiO_2	Minor components and inclusions
Olivines					
$(Mg_{2x}Fe_{2-2x}SiO_4)$					
x=1.0	forsterite (s)	56.2	-	43.8	0.2 CaO
x=0.94	olivine (n)	48.8	9.6	40.9	0.1 MnO_2, 0.4 NiO, 0.09 CaO
x=0.55	hortonolite (n)	19.5	44.1	34.7	1.4 MnO_2, inclusions:FeO,TiO_2
x=0.0	fayalite (s)	-	69.6	30.2	0.04 CaO
Pyroxenes					
$(Mg_xFe_{1-x}SiO_3)$					
x=1.0	clinoenstatite (s)	37.2	0.3	62.4	$<$1 CaO
x=0.96	enstatite (n)	36.2	2.1	60.7	0.9 Al_2O_3
x=0.88	bronzite (n)	34.1	6.0	59.0	0.4 MnO_2,Al_2O_3, CaO, inclusions:FeO,CrO_3,MgAlCr-silicates
x=0.65	hypersthene (n)	21.8	20.3	53.8	1.0 MnO_2, 0.8 TiO_2,Al_2O_3,1.5 CaO

roxenes also occur in meteorites. The most common Mg-Fe pyroxenes, the so-called orthopyroxenes, belong to the rhombic system. Orthopyroxenes with an FeO content between 5 and 15 mass % have the mineral name bronzite, orthopyroxenes with larger FeO content are called hypersthene. Ferrosilite does not occur as a natural mineral.

3. Synthesis and analytical characterization of the samples

Iron-free Mg silicate minerals are relatively sparse in nature. Therefore, we synthesized the pure end members $MgSiO_3$ and Mg_2SiO_4 in the laboratory. This was done by melting of SiO_2 and $MgCO_3$ in the right stoichiometric ratios. The melts were kept one hour at 1700 ^{o}C and then slowly cooled down (10^3 K/h) to room temperature. They crystallized very rapidly, so that a microcrystalline solid was formed.

Natural minerals often contain inclusions with completely different compositions. In a natural fayalite sample (Indonesia) we found a significant amount of inclusions consisting of sulfides and oxides of Fe, Cr, Ti and some other elements as well as separated phases of the iron silicate itself. For this reason, we prefered synthetic material to a natural mineral for spectroscopy. The synthetic fayalite was produced by melting a mixture of SiO_2 (silicon dioxide) and $FeC_2O_4{\cdot}6H_2O$ (iron oxalate) in the right stoichiometric ratio in an arc discharge furnace and cooling down the melt slowly to room temperature (10^3 K/h). Because of the tendency of the Fe^{2+} to be oxidized to Fe^{3+} during the melting and cooling, both processes were performed in an argon atmosphere. The synthesis of mixed Fe/Mg silicates of olivine or pyroxene composition in the way described for the pure magnesium and iron silicates leads to phase-separated (= inhomogeneous) materials.

Finally, we selected 8 samples of natural and synthetic pyroxenes and olivines, covering a wide range of Mg/Fe ratios (see Table 1). The analytical results are given in mass % of MgO, FeO, and SiO_2, a usual way to represent mass fractions of the single components present in minerals or synthetic materials. The use of the oxides does not mean that these are present as separate phases in the minerals. Only in the case of the inclusions are the oxides present as a separate phase. Among the samples five natural minerals, olivine, hortonolite, enstatite, bronzite, and hypersthene were studied. The actual composition of the natural minerals and synthetic materials and the homogeneity of the samples was proved by Scanning Electron Analysis (SEM) and Energy Dispersive X-ray analysis (EDX) of polished samples embedded in epofix resin. The EDX results have been confirmed by wet-chemical analyses of the olivine and forsterite samples. The determination of the Fe^{3+} content in the minerals was based on the procedure described in former papers (Jäger et al. 1994, Dorschner et al. 1995). The SEM investigations of the natural minerals have shown that they also contain minor amounts of additional oxides like CaO or MnO_2 and that most of them contain differently composed inclusions, which are given in the last column of Table 1. In all of our selected materials the inclusions are only minor components, so that all samples chosen for spectroscopic measurement are considered to be pure materials. In the case of the natural pyroxenes we detected a small amount ($<$ 5%) of weathered silicate material in the form of $Mg_3[(OH)_2/Si_4O_{10}]$ (talc) which must be homogeneously distributed in the samples. Additionally, the spectral influence of the inclusions was investigated by comparison of reflectance measurements of the inclusions by the microscope with the reflectance of the whole sample. We verified that they are minor components only and do not significantly influence the bulk spectra. However, we stress that in any case, it is important to check the spectral influence of the minor components in minerals used as laboratory analogues for cosmic dust.

The achievement of the thermodynamical equilibrium in the dust condensation zones of stars is not very probable (Nuth 1996, Frenklach 1997). Therefore, it is also interesting to investigate phase-separated materials in the olivine and pyroxene systems that also experienced non-equilibrium processes. Furthermore, new aspects of chemical processing of already formed silicates by heating and cooling processes in the interstellar medium and star-forming regions can be found by inves-

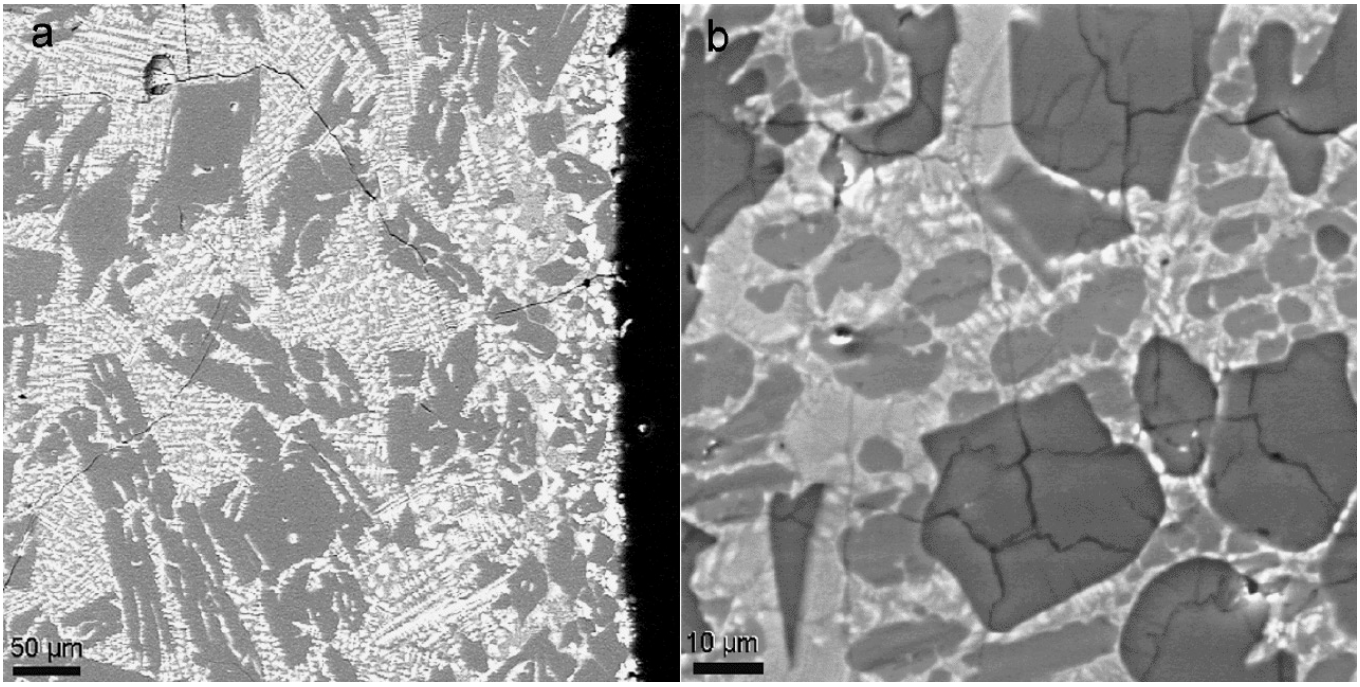

Fig. 1a and b. Scanning electron microscope images of the inhomogeneous olivine (**a**) and pyroxene (**b**). Explanation see text and Table 2.

Table 2. Analytical compositions of the inhomogenous silicate materials, determined by EDX analysis. The terms "dark", "gray", and "light" refer to the appearance of the corresponding phases in Fig. 1.

Phase	**Composition (mass %)**			**Phase characteriz.**
	MgO	FeO	SiO_2	
Olivine ($Mg_{1.5}Fe_{0.5}SiO_4$)				
dark	44.0	16.7	39.0	$Mg_{1.66}Fe_{0.34}SiO_4$
light	12.0	72.7	14.9	oxide-rich silicate
Pyroxene ($Mg_{0.4}Fe_{0.6}SiO_3$)				
dark	-	0.8	98.8	SiO_2 phase
gray	29.9	14.8	55.0	$Fe_{0.22}Mg_{0.8}SiO_3$
light	10.4	48.7	40.1	$Fe_{1.0}Mg_{0.39}SiO_{3.4}$

tigations of phase separations. Because of these astrophysical implications we also performed an extensive analytical characterization of such inhomogeneous samples. Fig. 1 shows the SEM micrographs of two selected materials of this type and Table 2 contains the analytical phase characterizations of them.

We found that the phase separations are much more frequent in synthetic pyroxene materials than in olivines. This is caused by the incongruent melting of pyroxene. This means, that for example a $MgSiO_3$ melt at liquidus temperature begins to crystallize to forsterite, and a SiO_2-rich melt remains, according to the chemical equilibrium (Matthes 1990)

$$2MgSiO_3 \rightleftharpoons Mg_2SiO_4 + SiO_2. \quad (1)$$

At 1557 °C, the so-called peritectic reaction between forsterite and SiO_2 begins, which means that the chemical equilibrium is shifted to the left side of Eq. (1), and all forsterite will be consumed. If the cooling is too rapid, the peritectic reaction cannot be completed. In this case forsterite, enstatite and cristobalite coexist in the crystallized mineral. As a matter of fact, these 3 minerals were found in our phase-separated synthetic pyroxenes. In contrast to the pyroxenes, olivines melt congruently, i.e. the melt and the crystallized phase have the same composition. Cooling an olivine melt too rapidly could lead to the zone crystallization in a Mg-rich and a Fe-rich olivine. This explains the occurence of only 2 phases. Additionally, the Fe^{2+} in the fayalite-rich component can be partially oxidized, leading to the formation of a rather Mg-rich olivine and to FeO and Fe_2O_3.

4. Spectroscopy

For transmission measurements small grains produced by grinding of the mineral samples and sedimentation in acetone were used to prepare KBr and polyethylene pellets. Spectroscopy was performed by means of a BRUKER 113v FTIR spectrometer in the wavenumber range from 5000 to 50 cm^{-1} (2-200 μm). In addition, the specular reflectance in the MIR range at nearly normal incidence was measured for the polished samples embedded in epofix resin. The MIR spectra of small inclusions and separated phases could be determined in the range from 5000 to 600 cm^{-1} (2-16.6 μm) by a microscope attached to the FTIR spectrometer. From the transmission spectra the mass absorption coefficients of the samples were derived. For the determination of optical constants of the natural enstatite, we performed reflectance measurements with IR radiation polarized parallel to the three crystallographic axes of the anisotropic

crystal. For this purpose we embedded pieces of a single crystal in an epofix resin providing the orientations necessary for the measurements. The surfaces were polished and checked by polarization microscopy and X-ray reflection measurements for the right orientation.

4.1. Olivines

In Fig. 2 we have plotted the MAC versus the wavelength for the different olivine samples. Obviously, the strengths of the bands at 10 and 20 μm relative to the underlying continuum decrease with increasing Fe content. With increasing Fe content, the structure in the spectra decreases and the bands become slightly broader in the wavelength region beyond 15 μm. Comparison of the spectra in Fig. 2 shows that with growing iron content the peaks will be shifted to longer wavelengths (see Sect. 3.3). Apart from the shift, peaks can disappear and new peaks can appear, depending on the Fe content. The peaks at 33.6 and 33.8 μm are clearly present in forsterite and olivine, respectively, but can only be observed as shoulders in hortonolite and disappear completely in fayalite. Generally, most of the FIR bands beyond 30 μm visible in the forsterite spectrum become very weak or disappear completely in the olivine and hortonolite samples. In contrast, fayalite shows two bands at 50.7 and 55.1 μm. The typical FIR peaks can be used to distinguish between pure Mg olivine and iron olivine in the silicate spectra of evolved stars.

We compared our results for the crystalline olivines with the results of Koike et al. (1993), Steyer (1974), Oehler & Günthard (1969), Paques-Ledent & Tarte (1973), and Hofmeister (1997). Steyer (1974) measured the reflectance spectrum of a natural crystalline olivine sample for the three crystallographic axes of the rhombic crystal system and evaluated the optical data. From these three data sets, he calculated the absorption efficiency Q, normalized to the particle size of a statistically oriented microcrystalline olivine material consisting of small spheres in the Rayleigh limit. This was done by averaging the absorption efficiencies according to $Q = 1/3(Q_a + Q_b + Q_c)$, where Q_a through Q_c are the efficiencies for the different axes. Additionally, he measured the transmission of olivine powder embedded in KBr up to a wavelength of 24 μm. He found some deviations between calculated and experimental data which were small in the 10 μm region, but became stronger between 15 and 25 μm. This disagreement could be caused by shape effects (non-spherical shape of olivine particles embedded in KBr), matrix effects, and by fundamental problem of mixing different crystallographic directions. The comparison of our olivine transmission data with his transmission measurements shows an excellent agreement in the number, positions, and shapes of the peaks. Unfortunately, Steyer did not analyze the chemical composition of his sample but the good agreement of the peak positions indicates that the compositions of the samples must be similar.

Koike et al. (1993) have measured transmission spectra of olivines in the range between 100 and 40 mass % forsterite content in the solid solution series of forsterite and fayalite. The peak positions for forsterite are shifted ($\leq$ 0.2 μm) to longer wavelengths compared to the measurements in this work. Our spectra show additional peaks at 9.3, 13.6, 13.8, 14.6, 18.3, 20.8, 24.7, 26.1, 43.3, 45.0, and 65.7 μm. For the other samples we found good agreement but again found additional peaks. A surprising point in the result of Koike et al. (1993) is the fact that their $Mg_{0.9}Fe_{0.1}SiO_4$ (olivine) spectrum peaks in the MIR at shorter wavelengths than their forsterite sample. As these authors already mentioned, this is in contrast to the general trend that a larger Fe content shifts the peaks to longer wavelengths. Our forsterite data are in a very good agreement with IR transmission data of Oehler & Günthard (1969) who studied a magnesium-rich olivine and with transmission data of Paques-Ledent & Tarte (1973), and Hofmeister (1997). The comparison to the latter work shows only minor differences in the region between 40-50 μm, where we find three additional bands of forsterite.

Hofmeister (1997) has also measured transmission data of a thin fayalite film and determined the dielectric function from reflection measurements of a single fayalite crystal. Our fayalite spectrum coincides very well with the transmission spectrum measured by Hofmeister, except for the small peak at 9.1 μm which could be caused by a minor component containing more SiO_2 than fayalite. In the scanning electron microscope we found no indication for the presence of such a component in the sample. However, it could be a phase separation on the nanometer scale.

In Table 3 the MAC peak positions of the different olivine samples are simply taken from transmission measurements without background correction. Since the peaks are very narrow we do not expect a peak shift due to a background absorption. The assignments of the bands to the vibrational modes given in Table 3 are mainly based on the results of Hofmeister (1997). The differences in the structure of olivines are the growing metal oxygen distances in the iron-rich samples (Birle et al. 1968), which cause the peak shift to longer wavelengths. Furthermore, the SiO_4 groups in olivines are distorted, which is also influenced by Fe incorporation. The broad and weak bands between 12.5 and 16 μm are assigned as overtones expected to occur at wavelengths between the Si–O stretching and bending modes (Hofmeister 1997).

4.2. Pyroxenes

In our samples the synthetic pure Mg silicate is of monoclinic structure, the other pyroxenes studied are all rhombic orthopyroxenes. Fig. 3 summarizes the mass absorption coefficients of the chosen synthetic and natural samples. Unfortunately we were not able to synthesize or to find sufficiently homogeneous pyroxenes with an iron content larger than *1-x=0.35* for the compositions $Mg_xFe_{1-x}SiO_3$.

The differences between the clino- and the orthoenstatite sample (see Fig. 3) result from a partial weathering of the natural pyroxenes which leads to the formation of a $Mg_3[(OH)_2/Si_4O_{10}]$ (talc) phase. This mineral has bands at 9.8, 14.9, 21.5, 22.2 μm. The Si-O stretching mode at 9.8 and the 21.5 μm band in the

Table 3. Peak positions in microns for different Fe/Mg ratios from the MAC spectra of olivines ($Mg_{2x}Fe_{2-2x}SiO_4$). Explanation of the symbols: s = strong, m = medium, w = weak, ? = very weak or doubtful, b = broad, sh = shoulder.

synthetical forsterite $x = 1$	natural olivine $x = 0.94$	natural hortonolite $x = 0.55$	synthetical fayalite $x = 0$	Comments
-	-	9.0sh	9.1m	
9.3m	-	-	-	
10.0s	10.0s	10.2s	10.4sh	asymmetric stretching ν_{as} of SiO_4
10.2sh	10.2sh	10.4?	10.6s	”
10.4m	10.5m	10.7m	10.9m	”
-	10.8w	-	-	”
11.2s	11.3s	11.3s	11.4s	”
11.9w	11.9m	12.0m	12.1m	symmetric stretching ν_s of SiO_4
-	-	13.2w	-	
13.6w	-	-	-	overtones
13.8m	-	-	-	overtones
14.6w	-	14.6?	-	overtones
16.3s	16.4s	17.0s	17.7m	asymmetric bending δ_{as} of SiO_4
18.3?	18.3w	19.1m	19.8m	”
19.5bs	19.5bs	20.5bm	21.0s	symmetric bending δ_s of SiO_4
20.8w	20.9w	-	-	rotation of SiO_4
21.5w	21.6w	-	26.6sh	”
23.5s	23.9s	25.5s	27.6bm	translation of one Me^{2+}
24.7w	25.3w	-	-	”
26.1m	26.4m	-	-	
27.5s	27.7s	28.4m	31.8bs	”
29.0?	-	-	-	
31.3m	-	-	-	”
33.5bs	33.8s	36.4w	39.5bw	”
36.3m	36.8sh	-	-	”
-	-	41.6w	-	”
40.7m	-	-	-	translation of one Me^{2+}
43.3m	-	-	-	
45.0w	-	-	-	translation of SiO_4
-	-	-	50.7w	translation of one Me^{2+}
49.8w	50.9w	51.8?	55.1w	translation of SiO_4
-	-	-	57.9sh	translation of one Me^{2+} and SiO_4
65.7w	-	-	-	translation of one Me^{2+} and SiO_4
69.7w	73.0w	84.4w	-	translation of one Me^{2+} and SiO_4
-	86.0bw		-	”

natural pyroxenes are superimposed on the talc bands, which are caused by the same vibrational modes providing an increase in their intensities. The weathering component talc is most abundant in the natural enstatite sample but it is also present in bronzite and hypersthene. The sedimentation process used to separate the small particles for spectroscopy enriched this component. This is due to the smaller density of talc compared to the pyroxene providing a lower sedimentation rate of the talc containing grains.

In general the pyroxene spectra show ratios of peak intensities to background absorption which are comparable to those of the olivines. The intensity of the maxima in the 10 and 20 μm regions decreases with decreasing Mg content and increasing Fe content in the samples. For example, the natural enstatite sample with 2.1 mass % FeO shows 6 peaks in the range between 9 and 12 μm and the prominent peak at 9.47 μm decreases in strength from 7200 to 1600 cm^2g^{-1} for the hypersthene sample with 20.3 mass % FeO. The same behaviour can be observed between 12 and 24 μm. There is also a shift of the peak positions to longer wavelengths depending on the iron content (see Sect. 4.3) and the longer Fe-O distances in the FeO_6 compared to MgO_6 octahedra, but not in the 10 μm region. In this region the peaks can be attributed to Si-O stretching modes which are not expected to be very sensitive to Fe incorporation. The peak positions and shifts of the bands of the the pyroxene samples can be found in Table 4. As in the case of the olivines, the positions of the peaks were simply taken from the transmission measurements. A background correction due to scattering was not necessary.

An exact attribution of peaks to vibrational modes of different structural groups is greatly complicated by the large number of atoms belonging to the unit cell, which is much larger for

Table 4. Peak positions in microns for different Fe/Mg ratios in pyroxene minerals ($Mg_xFe_{1-x}SiO_3$) from transmission measurements. Letters have the same meaning as in Table 3. Bands partly caused by $Mg_3[(OH)_2/Si_4O_{10}]$ (talc) occur only in the natural minerals enstatite, bronzite, and hypersthene.

syn. clinoenstatite	nat. orthoenstatite	nat. orthobronzite	nat. orthohypersthene	Comments
$x = 1$	$x = 0.96$	$x = 0.88$	$x = 0.65$	
8.7sh	8.7sh	9.2sh	9.0sh	
9.3bs	9.4s	9.4s	9.3sh	
-	-	-	9.5m	
9.9s	9.8s	9.8s	9.8m	blended with talc
10.35sh	10.32bs	10.5bs	10.4sh	
10.65s	10.65s	-	10.6bm	
11.1s	11.1m	11.1m	11.4bm	
11.6s	11.6m	11.6m	-	
13.6w	13.6sh	13.1w	-	
-	-	13.4sh	13.4w	
13.8w	13.8w	13.8w	13.8w	
14.5sh	14.5w	14.5m	14.6bw	
14.6w	14.9m	15.0m	-	due to talc (OH vibrations)
15.4m	15.4m	15.4bm	15.6bw	
17.6sh	17.7sh	17.7sh	18.0sh	
18.2s	18.5s	18.6m	18.8m	
19.3bs	19.4bs	19.8bs	20.0bm	
20.6m	20.7sh	20.7sh	-	
21.6m	21.5s	21.6m	21.6sh	blended with talc (OH vibrations)
21.9sh	22.0sh	22.3sh	22.1m	blended with talc
23.2bm	23.1w	23.1sh	-	blended with talc
-	23.4sh	-	-	
24.6w	24.5m	24.8m	24.7w	
-	25.4m*	-	25.8m	*due to talc
26.7bm	26.8m	27.0sh	27.0sh	
27.9bm	28.2bm	28.5bm	29.2bm	
29.0bm	29.6sh	29.8sh	-	
30.7sh	30.7sh	31.0sh?	30.7sh	
33.1w	33.2w	33.3w	-	
33.9w	34.0w	34.6w	-	
35.5bw	36.1bw	37.1m	-	
-	38.6sh	-	39.3sh	
40.8bw	41.4bw	-	-	
43.4bw	43.9bw	44.4bm	46.4bw	
48.1sh	49.3sh	50.0sh	51.9sh?	
51.4sh?	51.5sh	53.2?	58.1?	
-	-	64.0bw	64.9?	
-	-	71.4bw	-	
-	-	73.1bw	75.0bw	

pyroxenes than for olivines. Coupling of different vibrational modes is also possible. Peaks in the range between 8 and 13 μm originate from Si-O stretching vibrations of different SiO_4 tetrahedra due to distortions. The bands at 9.8, 21.5 and 22.2 μm are enhanced by the weathering component talc. The pure pyroxene spectrum can be derived from the mixed spectra by correction with a spectrum of talc which was done for enstatite. For this purpose the 14.9 μm peak only present in the talc spectrum was used as a criterion. The corrected enstatite spectrum can be seen in Fig. 5. In the region between 15-22 μm, bending vibrations of Si-O-Si links are expected. The peaks located at wavelengths longer than 17 μm can be attributed to the modes of MgO_6 and FeO_6 octahedra. We compared our measurements with the spectra of two magnesium-rich pyroxenes measured by Koike et al. (1993), and found good agreement of the bands in the 10 and 20 μm regions. However, due to better resolution at longer wavelengths, our spectra show more structural details.

4.3. Correlation between band shifts and Fe content

The peak positions of the olivine and pyroxene sample series are listed in Tables 3 and 4, respectively. From a statistical analysis of the band shifts, the following trends have been derived:

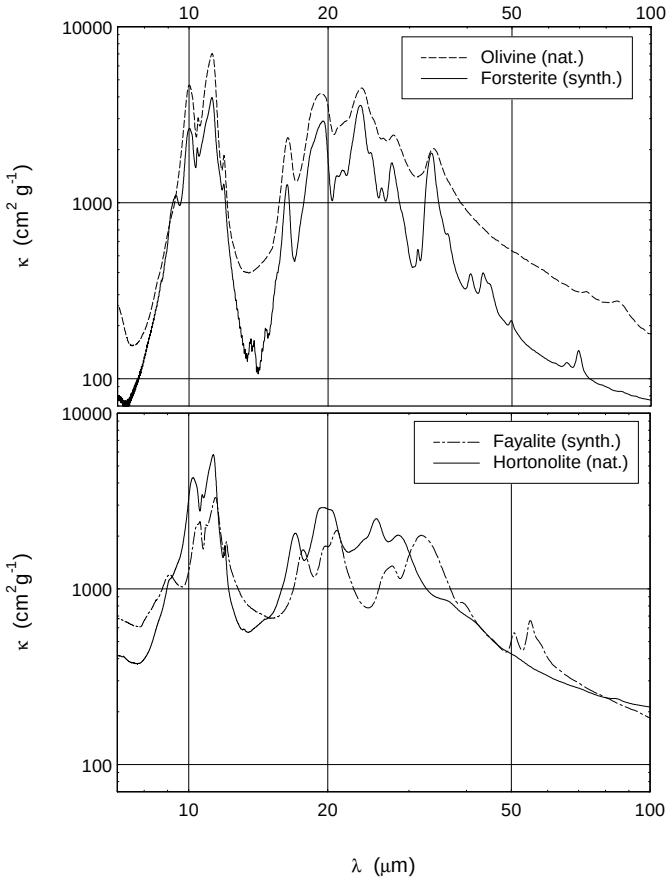

Fig. 2. Mass absorption coefficients calculated from transmission spectra for different olivine minerals.

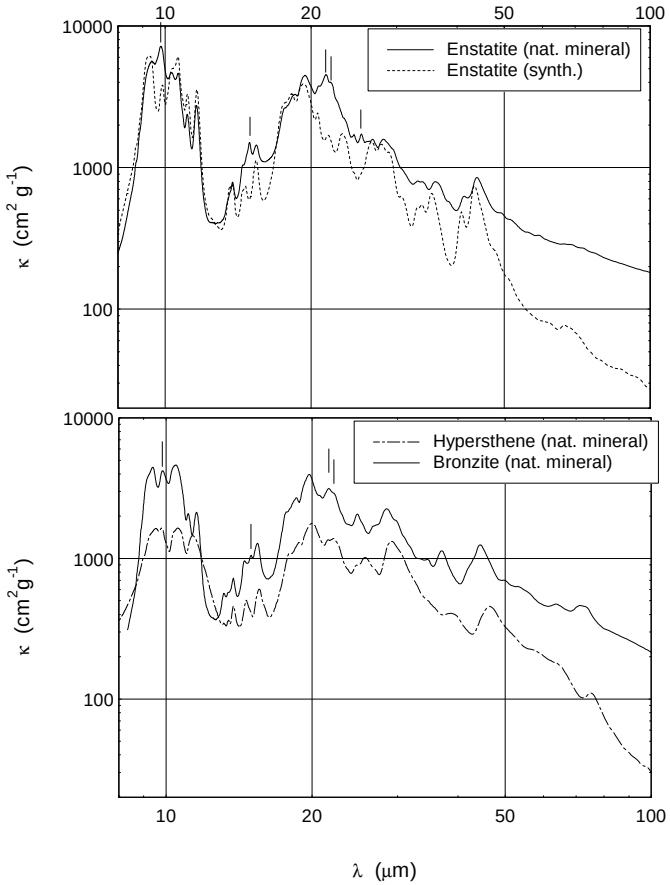

Fig. 3. Mass absorption coefficients calculated from transmission spectra for different pyroxene minerals. The vertical strokes mark the peaks which are superimposed by the $Mg_3[(OH)_2/Si_4O_{10}]$ (talc) phase.

1. All peaks of the olivine series are shifted towards longer wavelengths with growing Fe-content. The same trend is visible in the great majority of the bands of the pyroxene series. However, in the latter case there are a couple of exceptions, e.g. the band at 9.9 μm in the synthetic clinoenstatite spectrum. For the determination of $\Delta\lambda$, the Mg-rich end member was used as the zero-standard
2. For spectra plotted vs. wavelengths the shift $\Delta\lambda$ is proportional to λ^2. Since $-\Delta\nu$=$\Delta\lambda/\lambda^2$, this finding means that all bands are shifted by the same amount in wavenumber. Because of the statistical scatter of the data, this statement holds to within 20%.
3. The wavenumber shift $\Delta\nu$ is closely correlated with the Fe content (see Table 1). The correlation coefficient between the mass percentage of FeO ([FeO]) and $\Delta\nu$ amounts to 0.996 for olivines and 0.916 for pyroxenes. The relations for both sample series are: $[\mathrm{FeO}]/\Delta\nu = -1.8 \pm 0.1$ and $-1.5\pm$ 0.2 for olivines and pyroxenes respectively.

4.4. Optical data of enstatite

Two pieces of an enstatite single crystal have been cut and polished along the (001) (perpendicular to the c-axis) and (210) (parallel to the c-axis) crystallographic planes.

For these two samples we measured the specular reflectance of IR radiation polarized parallel to the crystallographic axes of the crystals (a- and b-axis with sample 1, c-axis with sample 2). Two wire grid polarizers on KRS-5 and polyethylene substrates, with a degree of polarization better than 95%, have been used to cover the wavelength range 2–100 μm. For the alignment of the plane of polarization to the crystallographic axes the accuracy is estimated to be about $\pm5^\circ$.

From the reflectance spectra, we obtained the complex refractive index[1] (Fig. 4) by Kramers-Kronig analysis as described in Jäger et al. (1994) and Dorschner et al. (1995). The differences between the polarization directions in Fig. 4 are striking. In each of the k-spectra there are strong bands which do not occur in the other spectra. Calculation of the mass absorption coefficients of Rayleigh particles of different shape distributions embedded in KBr/PE matrix (refractive index in both cases 1.52) and averaging of orientations gives the spectra shown in Fig. 5. The comparison with the measured powder spectra shows that there is a very good coincidence beween the calculated spectrum for CDE and the measured spectrum of orthoenstatite corrected for

[1] The n- and k-data files can be taken from the internet homepage of the Astrophysical Institute and University Observatory Jena (http://www.astro.uni-jena.de)

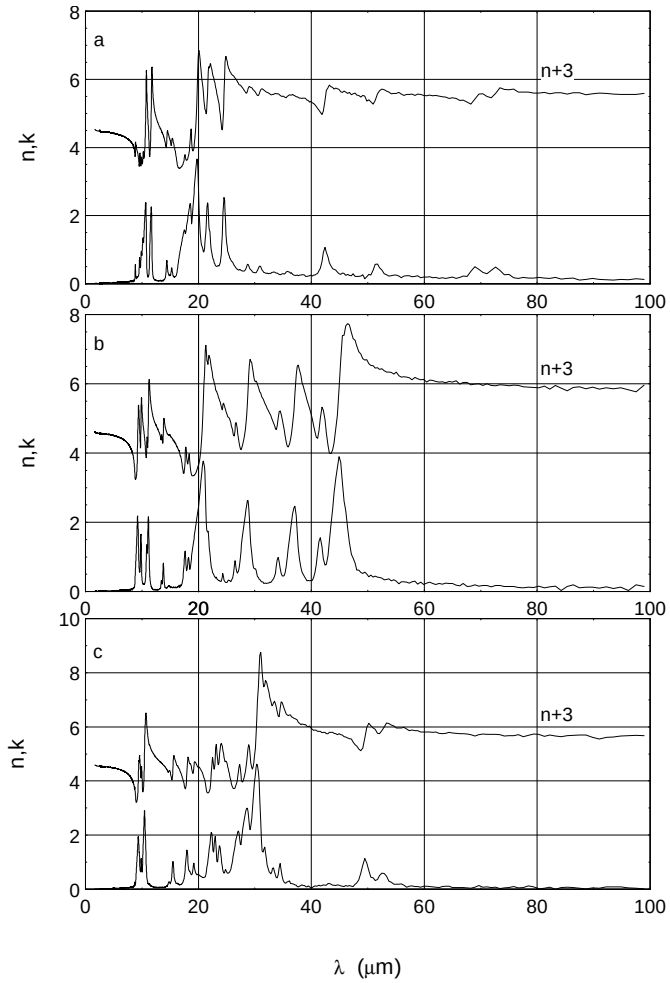

Fig. 4a–c. Complex refractive index n+ik for the three different crystallographic axes of the natural enstatite (**a** parallel to the c-axis; **b,c** perpendicular to the c-axis).

the talc bands, and also the clinoenstatite. Small deviations are probably caused by shape and size and agglomeration effects of the small grains embedded in KBr.

4.5. Non-homogeneous samples

In Fig. 6a,b we show the mass absorption coefficients of the two inhomogeneous pyroxene and olivine samples shown in Fig. 1 and Table 2 in comparison with a homogeneous material with similar Fe/Mg ratio. Surprisingly, the agreement between the inhomogeneous and homogeneous sample in the case of the olivine is quite good. In the inhomogeneous olivine sample, the spectrum is obviously dominated by the dark phase $Mg_{1.66}Fe_{0.34}SiO_4$ with a similar composition to natural olivine (see Table 2). For the inhomogeneous pyroxene material (see Fig. 6b) the differences are more pronounced compared to olivine, which is caused by the much lower total content of iron oxide in the homogenous sample in comparison to the phase-separated material and the formation of a larger number of different phases (see Sect. 3) during the cooling process

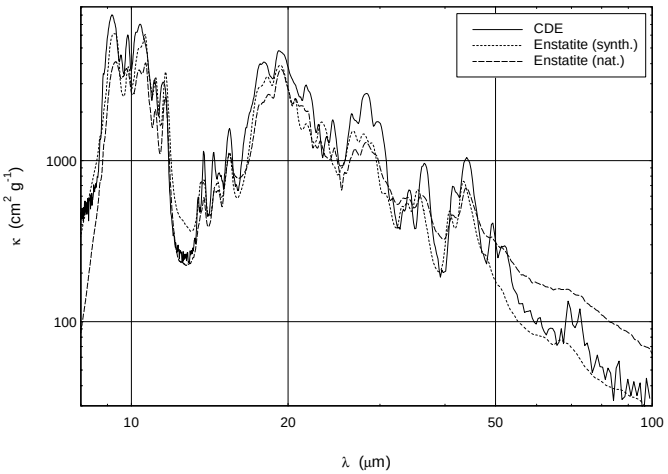

Fig. 5. The comparison of the absorption spectra calculated from the optical constants of natural enstatite for a CDE with the MAC spectra of the synthetic clinoenstatite and the natural enstatite. The spectrum of natural enstatite was corrected by the MAC spectrum of $Mg_3[(OH)_2/Si_4O_{10}]$ (talc).

of pyroxene melts. A better agreement for a pyroxene can be found in Fig. 6c, where another inhomogeneous material, with nearly the same composition as the homogeneous sample, are compared. The measured transmission spectra are the average of the transmission spectra of the different phases. The spectral behaviour of the various phases is demonstrated in Fig. 7, where we show microscopic reflection data of the separated regions. These reflection measurements provide some additional information necessary for the interpretation of changes in the transmission spectra. For example, the appearance of the shoulder at 9.2 μm in the transmission spectrum of the phase-separated olivine sample can be explained by an overlapping of the olivine component with the oxide-rich phase. In the mass extinction spectrum of the inhomogeneous pyroxene sample shown in Fig. 6b, a strong band at 9.1 μm is caused by the SiO_2-rich dark component. The peak at 20 μm typical of orthopyroxene is also overlapped by SiO_2 vibrations. The degree of spectral changes depends on the amount of SiO_2 phase present in the sample. For example, the inhomogeneous pyroxene sample in Fig. 6c contains less SiO_2 phase in comparison to the other inhomogeneous pyroxene material and that is why there is a better agreement between the homogeneous and heterogeneous material. Our investigations demonstrate that it is difficult to discriminate a homogeneous from a heterogeneous sample by IR spectroscopy.

5. Discussion

We compared our spectroscopic results with the astronomical data of the source AFGL 4106. AFGL 4106 is an evolved binary (Molster et al. 1998), which experienced a huge mass loss. Former IRAS-LRS measurements have shown that a large amount of amorphous silicates is present in the circumstellar shell. On 22 July 1996, ISO-SWS observed this object in an AOT01 speed 3 observing mode. The spectrum revealed the existence of a significant amount of crystalline silicates. For comparison with

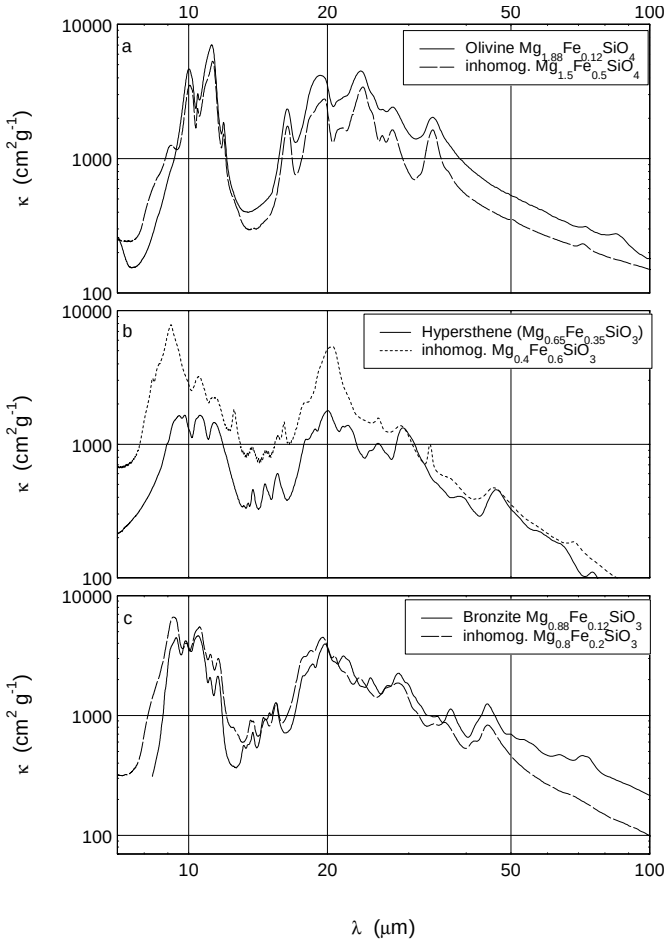

Fig. 6. a and **b** show a comparison of the mass absorption coefficients for two inhomogeneous synthetic samples (see Fig. 1 and Table 2) of olivine and pyroxene composition, respectively, with the corresponding homogeneous materials. **c** presents another inhomogeneous pyroxene sample with a composition more similar to the homogeneous bronzite material, which shows a good agreement between the two spectra.

our laboratory data we subtracted a kind of continuum from the ISO-SWS spectrum. The result of this procedure is plotted in Fig. 8. In the same figure we show normalized MAC multiplied by a 100 K Planck function. The dust temperature of 100 K is a very rough estimate of the mean dust temperature of the object. The relative strength of the bands in the spectrum is sensitive to the temperature of the dust, which can be easily seen by a comparison with the spectra in Figs. 2 and 3.

Although there is a good agreement between the continuum-subtracted spectrum of the source AFGL 4106 and the laboratory data of forsterite, not every peak in the spectrum can be matched. Quite a number of the remaining peaks can be fitted with synthetic enstatite (see Fig. 8). We found that only the very magnesium-rich crystalline silicates can explain the spectrum of AFGL 4106. The 69.7 μm feature, which is present in some other sources is unfortunately too weak to be detected in this source. This band is a suitable indicator for the presence of very Mg-rich crystalline olivines (see Sect. 3).

Also in our own planetary system there is ample evidence for the existence of crystalline silicates like in the spectrum of comet Hale-Bopp (Crovisier et al. 1997). A detailed comparison of the emission features between 6 and 45 μm with the silicate spectra presented in this paper supports the presence of a magnesium-rich olivine (forsterite) additional to an amorphous silicate component.

Laboratory IR transmission spectra of individual dust particles (Sandford & Walker 1985) collected in the stratosphere also show the occurrence of a wide variability of crystalline olivines and pyroxenes. However there is no indication for a larger abundance of the pure Mg silicate materials like forsterite or enstatite.

Still there are some differences between the ISO-SWS spectrum and the laboratory measurements, in the width, strength, and position of some of the features. Differences in width can be caused by differences in size and shapes of the grains. Despite our efforts to produce small grains, coagulation could have taken place during the production of the pellets used for the transmission measurements. It is quite unrealistic to assume that the grinding process produces the same grain shapes as are present in circumstellar outflows. Differences in strength can be partially explained by the fact that there is a temperature distribution instead of one single temperature. In addition, we have to keep in mind that the ISO-SWS spectrum shown here consists of five independent spectra of different wavelengths regions. Although we took pains to attach the different spectra correctly to each other, it still remains a source of uncertainty in the occurrence and strength of some features, especially those situated near the edges of the spectral regions. Discrepancies in the peak positions are not easy to explain by matrix effects of KBr or PE. Calculations of the absorption behaviour of spheres in the Rayleigh limit, with the optical data of olivine determined by Steyer (1974), in a KBr matrix and vacuum, have shown that there are shifts of different band centres ranging from 0 to 0.6 μm to longer wavelengths for the sample embedded in KBr/PE. Additionally, we found differences in shapes and peak strengths. However, the formation of exactly spherical grains in the circumstellar outflow is not expected. An approach more realistic than the spheres would be the calculation of the absorption efficiency of a continuous distribution of ellipsoids (CDE) (Bohren & Huffman 1983). We show the result of these calculations in Fig. 9. It demonstrates that there is no change in the peak positions for the different matrices, but the intensity of the peaks in KBr is about 1.4 times higher than in vacuum over the whole wavelength range. Since only very limited information about shape and size distributions of interstellar silicate grains is available it is very difficult to quantify matrix and shape effects in order to compare laboratory and astronomical spectra in an appropriate manner.

Mindful of all considerations mentioned before, we want to point out that there are some bands that are unexplainably strong, like those at 20.6, 21.5, 26.1 and the plateau from 30 to 45 μm. It is also likely that other materials are present in the circumstellar shell, for example Fe-containing oxides, Ca-containing silicates, sulfates and H_2O ice.

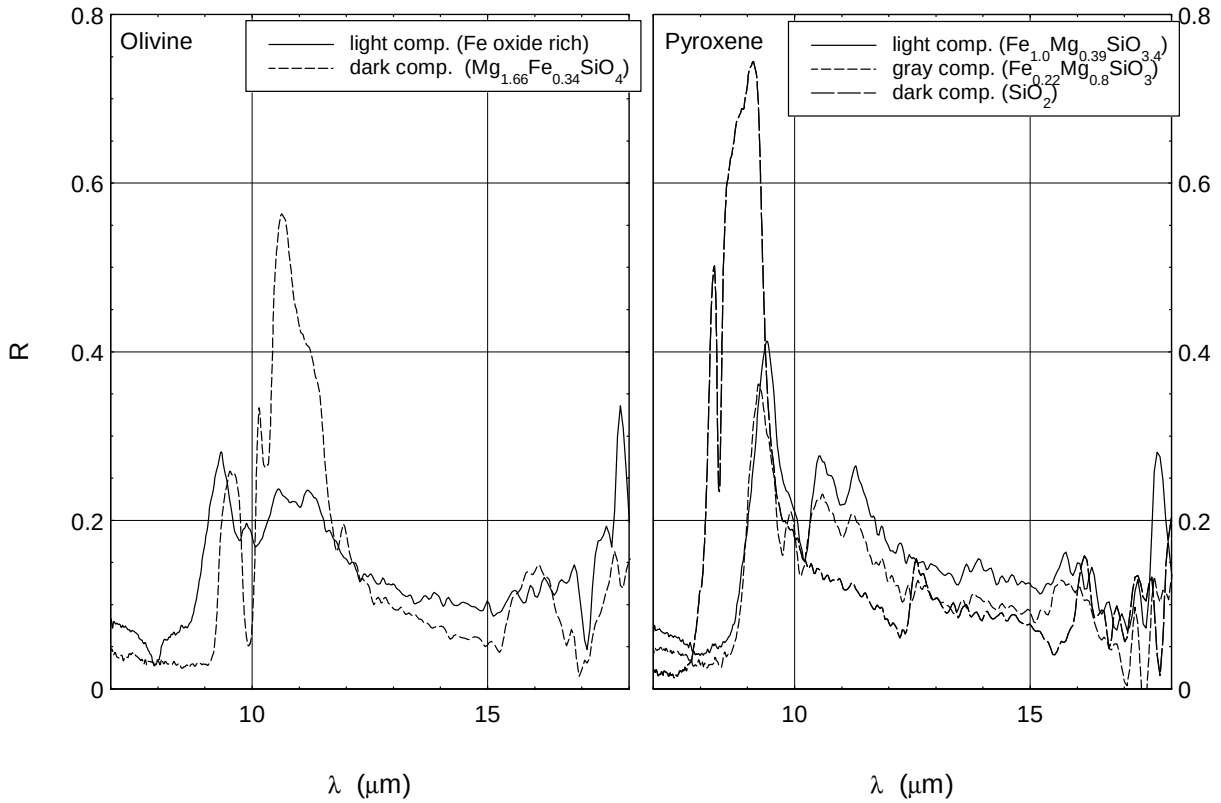

Fig. 7. Microscope reflection measurements of the different phases in the inhomogeneous samples shown in Fig. 1.

The details of silicate dust formation in oxygen-rich shells are still unknown. First ideas were based on thermodynamical equilibrium considerations of non-homogenous nucleation postulating condensation sequences (Tielens et al. 1990). More recent investigations found a lot of indications for incomplete condensation and dust formation as a non-equilibrium process. One indication is for example the detection of SiO molecules in the outer regions of circumstellar shells. Based on laboratory experiments, Nuth (1996) described grain formation as a complex process starting with the nucleation of SiO and formation of SiO_x clusters. Other underoxidized species like AlO_x, FeO_x and MgO and metallic components are also formed, which can react in internal oxidation/reduction reactions forming an underoxidized low-density silicate material, a so-called "chaotic" silicate. Three phases, forsterite, enstatite and SiO_2 were also found in experimentally produced Mg-SiO smokes (Rietmeijer et al. 1986) as one form of chaotic silicate material. This demonstrates that the same phase separations could take place in the chaotic silicates described by Nuth & Hecht (1990) and in inhomogeneous samples produced by cooling of molten material (discussed in this paper). It is interesting to see that different starting materials provide the same products and phase separations.

One remaining question is how the crystalline material is formed in circumstellar shells and what we can say about chemical processing and aging of silicate dust during the transition from the circumstellar environment to the interstellar medium and the star-forming regions. Crystalline dust features are prominent in the ISO SWS spectra of stars on the Asymptotic Giant Branch (AGB) and those of Red Supergiants, if the color temperature of the dust is low (typically less than 200-300 K). A low color temperature for stars with dusty outflows corresponds to high dust optical depth, and thus with high mass loss rates. There are indications that the crystalline dust features are more prominent in post-AGB stars and planetary nebulae (PNe), suggesting perhaps an increase in the abundance of crystalline silicates. The dust shell in post-AGB stars and PNe, which is the remnant from the high mass loss phase on the AGB, expands and cools to temperatures below 100 K.

Hallenbeck et al. (1998) have observed that annealing of amorphous magnesium silicate smoke at temperatures slightly above 1000 K for more than 10 h causes remarkable changes of the profile of the 10 μm band, which indicate internal ordering processes of the arrangement of atoms leading to crystalline structures. According to this results the requirement for the crystallization process is a sufficient high temperature ($\geq$ 900 K) and/or a corresponding annealing time. Recently, Gail and Sedlmayer (1998) have shown that corresponding conditions for annealing processes are given in M giants. Clearly, many questions concerning the origin and evolution of crystalline dust in the outflows of evolved stars remain open.

A related issue is the apparent absence of crystalline silicates in the interstellar medium (ISM). This suggests that crystalline silicates are not produced with sufficient abundance in the outflows of evolved stars to be detectable, or they are destroyed in the ISM. The high abundance of Mg-rich crystalline silicates in

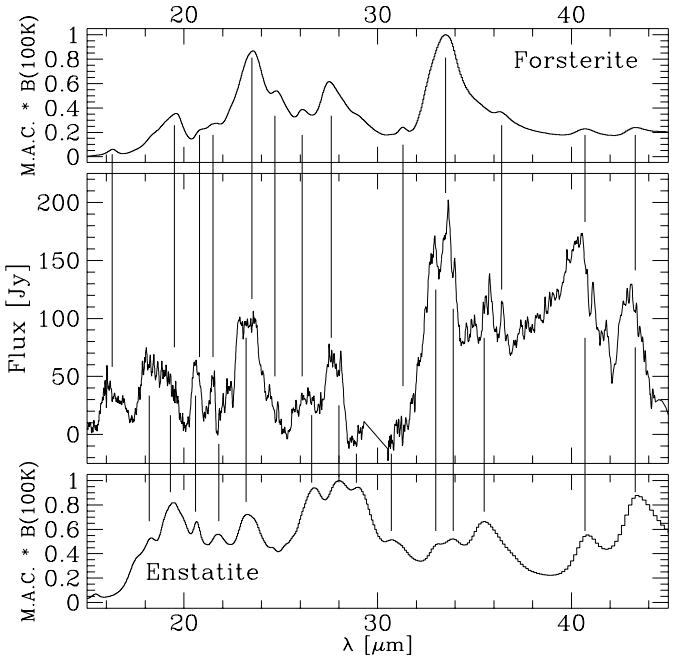

Fig. 8. Comparison of the continuum subtracted spectrum of AFGL 4106 with the MAC of forsterite and clinoenstatite multiplied by a Planck curve of 100 K and normalized to one.

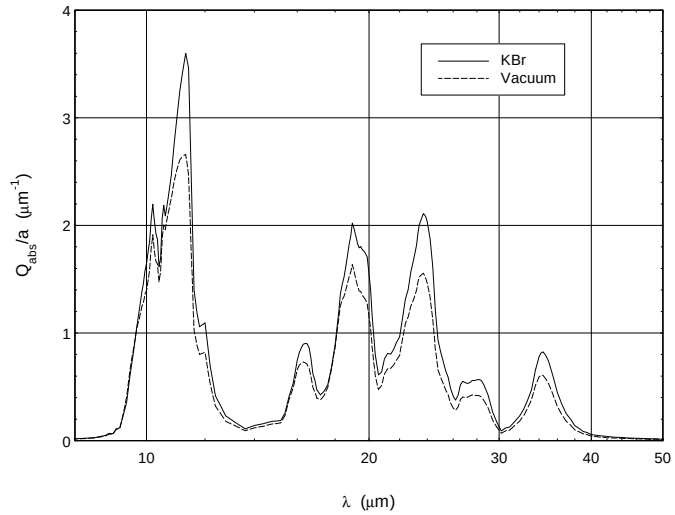

Fig. 9. Comparison of the calculated absorption efficiency of a CDE in KBr and in vacuum from the optical constants of olivine (Steyer 1974).

some young stars (Malfait et al. 1998) suggests that such grains are produced during the star formation and planet formation process, from annealing of amorphous grains.

In this paper we have demonstrated that crystalline Mg-rich silicates are responsible for the observed sharp peaks at longer wavelengths in the oxygen-rich circumstellar environments seen in the ISO spectra. We consider this as one of the most important findings of the ISO mission.

References

Aitken D.K., Smith C.H., James S.D., Roche P.F., Hough J.H. 1988, MNRAS 230, 629

Bradley J.P., Humecki H.J., Germani M.S. 1992, ApJ 394, 643

Birle J.D., Gibbs G.V, Moore P.B., Smith J.V. 1968, Amer. Mineral. 53, 807

Bohren C.F, Huffman D.R. 1983, *Absorption and scattering of light by small particles.*, John Wiley and Sons, Inc., New York

Bregmann J.D., Campins H., Witteborn F.C., et al. 1987, A&A 187, 616

Burns R.G. 1970, Amer. Mineral. 55, 1608

Cohen M., Witteborn F.C. 1985, ApJ 294, 345

Crovisier J., Leech K., Bockelee-Morvan D., et al. 1997, Science 275, 1904

Dorschner J. 1997. In: Greenberg, J.M., Kerridge, J.F. (eds.), *Formation and Evolution of Solids in Space*, Kluwer, Dordrecht, in press

Dorschner J., Henning Th. 1986, Ap&SS 128, 47

Dorschner J., Henning Th. 1995, A&AR 6, 271

Dorschner J., Begemann B., Henning Th., Jäger C., Mutschke H. 1995, A&A 300, 503

Fajardo-Acosta S.B., Knacke R.F. 1995, A&A 295, 767

Frenklach M. 1997. In: Pendleton Y.J. and Tielens A.G.G.M. (eds.), *From stardust to planetesimals*, pp 107-118, A.S.P. Conf. Ser. Vol. 122, San Francisco

Gail H.-P., Sedlmayr E. 1998. In: Hartquist T.W. and Williams D.A. (eds.), *The molecular astrophysics of stars and galaxies–A volume honouring Alexander Dalgarno*, Oxford University Press, Oxford, in press

Hallenbeck S. L., Nuth III J.A., Daukantas P.L. 1998, Icarus 131, 198

Hanner M.S. 1996. In: Gustafson B.Å.S, Hanner M.S. (eds.), *Physics, Chemistry, and Dynamics of Interplanetary Dust*, pp 367-376, A.S.P. Conf. Ser. Vol. 104, San Francisco

Hanner M.S., Lynch D.K., Russell R.W. 1994, ApJ 425, 274

Henning Th., Mutschke H. 1997, A&A 327, 743

Hofmeister A.M. 1997. Phys. Chem. Minerals, 24, 535

Jäger C., Mutschke H., Begemann B., Dorschner J., Henning Th. 1994, A&A 292, 641

Justtanont K., De Jong T., Helmich F.P., et al. 1996, A&A 315, L217

Kessler M.F., Steinz J.A., Anderegg M.E. et al. 1996, A&A 315, L27

Knacke R.F., Fajardo-Acosta S.B., Telesco C.M., et al. 1993, ApJ 418, 440

Koike C., Shibai H., Tuchiyama A. 1993, MNRAS 264, 654

Kovach J.J., Hiser A.L., Karr C. 1975. In: Karr C., Jr. (ed.), *Infrared and Raman Spectroscopy of Lunar and Terrestrial Minerals*, pp 325-358, Academic, New York

Liese H.C. 1975. In: Karr C., Jr. (ed.), *Infrared and Raman Spectroscopy of Lunar and Terrestrial Minerals*, pp 325-358, Academic, New York

Mackinnon I.D.R., Rietmeijer F.J.M. 1987, Rev. Geophysics 25, 1527

Malfait K., Waelkens C., Waters L.B.F.M., et al. 1998, A&A, 332, L25

Matthes S., 1990, *Mineralogie*, Springer-Verlag, Berlin Heidelberg

Molster F.J., Waters L.B.F.M., Trams N., et al. 1998. In: Waters L.B.F.M., Waelkens C., van der Hucht K.A., Zaal P.A. (eds.), *ISO's view on stellar evolution*, Kluwer, Dordrecht, in press

Mutschke H., Begemann B., Dorschner J., et al. 1998, A&A 333, 188

Nuth J.A. 1996. In: Greenberg J.M. (ed.), *The Cosmic Dust Connection*, pp 205-221, Kluwer, Dordrecht

Nuth J.A., Hecht J.H. 1990, A&SS 163, 79

Oehler O., Günthard H.H. 1969, J. Chem. Phys. 51, 4719

Paques-Ledent M.Th., Tarte P. 1973, Spectrochim. Acta 29A, 1007

Rietmeijer F.J.M., Nuth J.A., Mackinnon I.D.R. 1986, Icarus. 66, 211-222

Sandford S.A., Walker R.M. 1985, ApJ 291, 838

Steyer T. R. 1974, PHD-thesis, University of Arizona

Tielens A.G.G.M 1990, In: Menessier M.O., Omont A. (eds.), *From miras to planetary nebulae*, pp 186-200, Editions Frontièrs, Gif sur Yvette Cedex

Waelkens C., Waters L.B.F.M., De Graauw M.S., et al. 1996, A&A 315, L245

Waters L.B.F.M., Molster F.J., de Jong T., et al. 1996, A&A 315, L361

Waters L.B.F.M., Morris P.W., Voors R.H.M., Lamers H.J.G.L.M. 1997. In: A. Nota & H.J.G.L.M. Lamers (eds.)*Luminous Blue Variables: massive stars in transition*, pp 326-331, ASP Conf. Series vol 120,

White W.B. 1975. In: Karr C., Jr. (ed.) *Infrared and Raman Spectroscopy of Lunar and Terrestrial Minerals* pp 325-358, Academic, New York